Magnetotransport characterization of THz detectors based on plasma oscillations in submicron field effect transistors

© *J. Lusakowski* *,**, *W. Knap* *,****, *N. Dyakonova* *, *E. Kaminska* ***, *A. Piotrowska* ***, *K. Golaszewska* ***, *M.S. Shur* ****, *D. Smirnov* *****, *V. Gavrilenko* ******, *A. Antonov* ******, *S. Morozov* ******

* GES–UMR, CNRS–Université Montpellier 2,
34950 Montpellier, France
** Institute of Experimental Physics, University of Warsaw,
00-681 Warsaw, Poland
*** Institute of Electron Technology,
02-668 Warsaw, Poland
**** Rensselaer Polytechnic Institute, Troy,
N.Y. 121180-3590, USA
***** Ioffe Institute, Russian Academy of Sciences,
194021 St. Petersburg, Russia
****** Institute for Physics of Microstructures, Russian Academy of Sciences,
603950 Nizhnii Novgorod, Russia

E-mail: gavr@ipm.sci-nnov.ru

Magnetotransport characterization of field effect transistors in view of their application as resonant detectors of THz radiation is presented. Three groups of different transistors based on GaAs/GaAlAs or GaInAs/AlGaAs heterostructures in investigated at liquid helium temperatures and for magnetic field up to 14 T. The magnetic field dependence of the transistor's resistance is used for evaluation of the electron density and mobility in the transistor's channel. The electron mobility and concentration determined from magnetotransport measurements are used for the interpretation of recently observed resonant detection of terahertz radiation in 0.15 μm gate length GaAs transistors and for the determination of the parameters of other field effect transistors processed for resonant and voltage tuneable detection of THz radiation.

The terahertz part of the electromagnetic spectrum lies at the border between wavelengths generated by solid state electronics and optics. Many excitations observed in condensed matter, liquids, gases and biological substances correspond to the THz range of frequincies, i. e. to $\sim 0.3-30$ meV photon energies. Spectral analysis in the THz region can be used for studies of these excitations, such as phonons, cyclotron or spin resonance, as well as for investigations of molecular (rotational and vibrational) excitations in liquids, gases and biological substances. A growing interest in the analysis of signals carried by THz radiation is also related to possible applications of THz spectroscopy for non-destructive sensing and imaging in medicine, food industry and defence [1,2].

Terahertz broadband detectors include bolometers [3–5], pyroelectric detectors, Schottky diodes [6,7] and photo-conductive detectors [8]. An advantage of selective and tuneable detectors is that they require no gratings of moving mirrors of perform a spectral analysis. Tuneability was demonstrated for photoconductive detectors (GaAs [9], InP [10], and InSb [11]) placed in a magnetic field which tuned the energy of optical transitions between the levels of shallow donors or cyclotron and impurity shifted cyclotron resonance. Such detectors, however, require liquid helium temperatures and magnetic fields of a few Tesla.

For many applications, tuning a detector's response with an applied voltage is much easier than by the magnetic field.

A resonant, voltage-tunable detection based on excitation of plasmon resonance in a two-dimensional electron gas (2 DEG) confined in a field effect transistor (FET) was proposed in the early 90-es [12,13], and reported only recently [14–16]. A FET, biased by gate-to-source voltage U_{gs}, and subject to and electromagnetic radiation can develop a constant drain-to-source voltage U_{ds}, which has a resonant dependence on the frequency of radiation with maxima at plasma oscillation frequencies [12], $f_N = \omega_N/2\pi$. Resonant plasma frequencies are discrete and given by $\omega_N = \omega_0(1 + 2N)$, where $\omega_0 = \pi s/2L$, and $N = 0, 1, 2 \ldots$. The plasma wave velocity, s, depends on the carrier density in the transistor's channel, n, and the gate-to-channel capacitance $(C = \varepsilon\varepsilon_0/d)$ per unit area: $s = (e^2 n/mC)^{1/2}$, where e and m are the electron charge and the effective mass, respectively, ε is dielectric constant and d is the gate-to-channel distance. In the gradual channel approximation, the carrier density in the channel is related to the gate-to-source voltage by a relation $n = CU_0/e$, where U_0 is the gate-to-channel voltage swing, $U_0 = U_{gs} - U_{th}$, and U_{th} is the threshold voltage. The fundamental plasma frequency can be expressed by an approximate relation

$$f_0 = \frac{1}{4L}\sqrt{\frac{eU_0}{m}}. \qquad (1)$$

This has two important consequences: i) a sufficiently short (sub-micron) FET can operate as a THz detector and
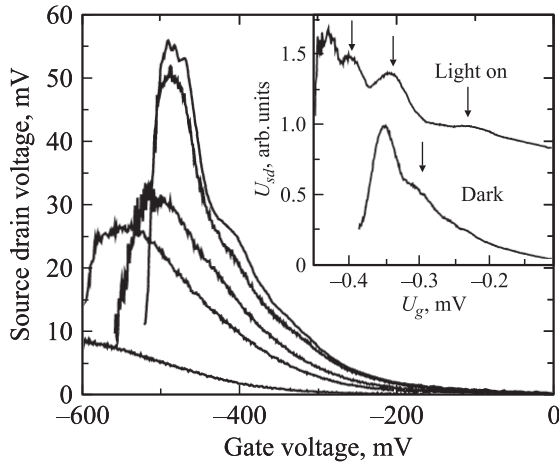
Figure 1. Photoinduced drain-to-source voltage of GaAs/GaAsAs FET (from group *A*) as a function of gate-to-source voltage and temperature from 8, 20, 60, 100 K to 200 K (from top to bottom). Inset shows the resonant detection of the 0.6, 0.8 and 1.2 THz radiation from multiplied Gunn diode source (See [14] and [17] for details). Higher Gunn diode harmonics are visible after illumination of FET [15]. The arrows mark positions of 2D plasmon resonances — and corresponds to detection of 0.6, 0.8 and 1.2 THz from left to the right correspondingly (See [14] and [15] for details).

ii) a pesponse frequency of such a detector can be tuned by gate-to-source voltage.

The width of a resonant curve is determined by the quality factor $\omega_0\tau$, wher τ is the electron momentum relaxation time. The resonant detection becomes possible if the quality factor reaches and exceeds the value of 1. If $\omega_0\tau \ll 1$, plasma oscillations are over-damped and the FET response is a smooth function of ω as well as of gate-to-source voltage (a non-resonant broadband detection [17]).

Resonant and non-resonant detection of THz radiation was recently demonstrated in two field-effect devices: a commercial FET [14,15,17] and a double quantum well FET with a periodic grating [16]. In both cases, the frequency of a standing 2D plasmon wave was tuned to a THz frequency by varying the gate-to-source voltage. In Fig. 1 we show an example of the resonant detection of THz radiation rerformed using a GaAs/GaAlAs FET.

The temperature evolution of spectra shown in Fig. 1 is mainly related to a change in the electron scattering time. A resonant feature (marked by an arrow) starts to be visible below about 30 K because only then does th electron scattering time increases sufficiently for the condition $\omega_0\tau \gg 1$ to be fulfilled. Illumination of the transistor with visible light leads to an additional increase of the electron mobility (μ) and, as a result, to an increase of the quality factor $\omega_0\tau$. This allowed for better resolution of the main resonance (0.6 THz) and observation of the resonant detection of higher harmonics (0.8 and 1.2 THz) of a frequency-multiplied 0.2 THz Gunn diode source — as shown in the inset in Fig. 1.

The most important parameters related to the resonant detection are the electron scattering time and the electron concentration. The former one, related to the electron mobility, enters into the quality factor $\omega_0\tau$, which, for given value of τ, gives a low bound of frequency for which FET can operate as a resonant detector. The electron concentration determines the transistor threshold voltage (which affects the maximum swing voltage, directly related to the frequency of plasmon resonance, as shown in Eq. 1). Therefore, determination of the electron density and mobility in a transistor is a key point in view of its applications as a resonant plasma device. The magneto-transport determination of these parameters is addressed in the present work.

The standard equations for the current density (j) in the 2DEG in the presence of the magnetic field (perpendicular to the 2DEG plane) are

$$j_x = \sigma_{xx}E_x + \sigma_{xy}E_y,$$

$$j_y = -\sigma_{xy}E_x + \sigma_{xx}E_y.$$

Here E_x and E_y are the components of the electric field in the (xy) plane and σ_{xx} and σ_{xy} are components of the comductivity tensor. In the Drude–Boltzman theory these components depend on the magnetic field:

$$\sigma_{xx} = \sigma_0/(1 + \mu^2 B^2),$$

$$\sigma_{xy} = \sigma_0\mu B/(1 + \mu^2 B^2).$$

The boundary conditions for these equations depend on the sample geometry. Two important limiting cases considered in this work are the Hall bar geometry and „transistor geometry" (with the device width, D, being much larger than the device length, L). For a long Hall bar, $L \gg D$. In this case, there is no current in the „y" direction, $j_y = 0$, and the measured $E_x = j_x/\sigma_0$. This means that conductivity (and resistivity) does not depend on the magnetic field. In other words there is no magnetoresistance. This is a general feature of a degenerate two-dimensional gas. On the other hand, in the case of a very short but wide device ($L \ll D$), the Hall voltage is short-circuited by long current-supplying contacts. Then $E_y = 0$ and $j_x = \sigma_{xx}E_x$. This geometry is equivalent to that of the Corbino disk. In this case, the measured $E_x = j_x(1 + \mu^2 B^2)/\sigma_0$ and one expects a parabolic increase of the sample resistance and Lorentzian $(1/(1 + \mu^2 B^2))$ decrease of the conductance. The coefficient of the parabolic magnetoresistance (or halfwidth or Lorentzian magnetoconductivity) is equal to the mobility. In quantizing magnetic fields ($\mu B \gg 1$), the conductivity exhibits Shubnikov–de Hass oscillations. These oscillations are periodic as a function of inverse magnetic field ($1/B$), the period depending only on the carrier density.

In this work, different GaAs and GaInAs FETs and Hall-bar test structures were investigated by magnetotransport measurement in high magnetic field (up to 14 T). We show how magnetoconductivity data allow evaluating the electron

mobility and concentration in a transistor channel even for a non-ideal geometry. The results are then used for the interpretation of the recently observed resonant detection and for the estimation of the parameters relevant to the THz detection in these field effect transistors. The maximun frequency and the quality factor that limit the THz detection in different field effect structures are descussed.

1. Experiment and Results

Three groups of devices, named A, B and C, were investigated. The group A included commercially available Fujitsu FX20 FETs with a gate length (L) of 0.15 μm, gate width (D) of 50 μm and the gate to channel separation (d) of $\sim$ 25 nm. Their threshold voltage varied between –0.2 and –0.5 V and the electron mobility was estimated to be 0.1–0.2 m^2/Vs at 300 K and 0.5–1.0 m^2/Vs at 4 K.

Transistors and Hall-bars of the group B and C were processed out of MBE-grown high electron mobility GaAs/GaAlAs and GaInAs/GaAlAs heterostructures, respectively. The group B transistors had the threshold voltage of –0.2 to –0.5 V and the electron mobility of 5–20 m^2/Vs at 4.2 K, while the corresponding values for the group C transistors were –1 to –2 V and 1–2 m^2/Vs, respectively. The gate to channel distance was $d \sim 160$ and $d \sim 40$ nm for group B and C transistors, respectively. The same mask was used in the case of B and C (Fig. 2) which defined transistors with the gate length equal to 0.8, 1.5 and 2.5 μm. The source to drain distance was 10 μm for all transistors and the gate was placed close to the source contact to ensure asymmetry of the transistor (necessary for the detection). Two gated Hall-bars and a Schottky diode were fabricated next to each group of the six transistors. Hall structures
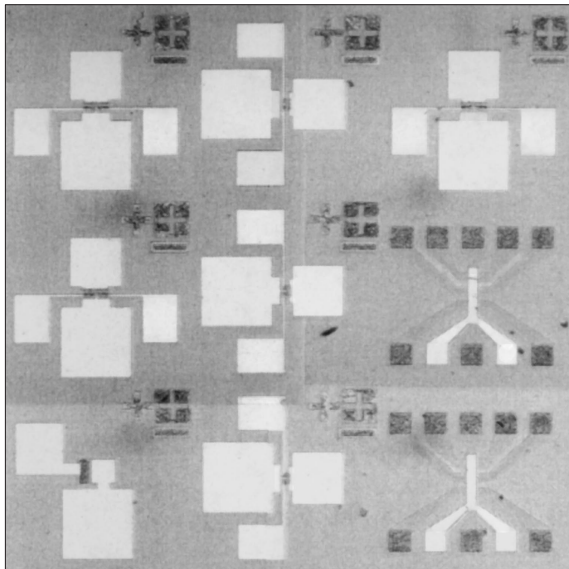

Figure 2. A photograph of a dice of the group B and C devices with litographically defined six transistors, two Hall-bars and Schottky diode.
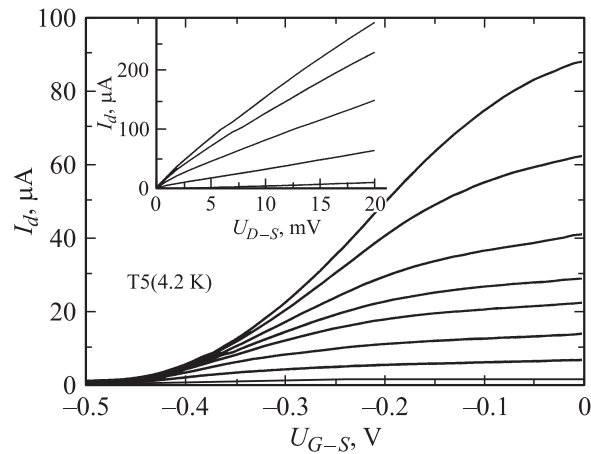

Figure 3. Example of characteristics of transistor T5 (from group B). Transient characteristics at $T = 4.2$ K as a function of the magnetic field, B, equal to (from top to bottom, in Tesla): 0, 0.030, 0.051, 0.068, 0.090, 0.140, 0.260 and 1. The inset shows output characteristics for gate-source voltage equal to (from top to bottom, in volts): 0, –0.1, –0.2, –0.3 and –0.4.

were used for independent measurements of the electron density and mobility.

Measurements were carried out at liquid helium temperatures (4.2 or 8 K) after cooling the sample in the dark. A typical set of measurements carried out on transistors involved: i) output characteristics (drain current, I_d, vs. drain-to-source voltage, U_{ds}) as a function of U_{gs} voltage and the magnetic field, B; ii) transient characteristics (drain current vs. gate-to-source voltage, U_{gs}) as a function of B; iii) magnetoconductivity (drain current vs. B) as a function of gate-to-source voltage. (Let us note that in the following the gate-to-sourse voltage is always negative and its increase means an increase of its absolute value.) An example of the experimental data, for one of the group B transistors, is shown in Fig. 3.

In some cases, additional data were taken after illumination of a sample with a red light emitting diode. Output characteristics were used for determination of a range U_{ds} and U_{gs} which drain current changed linearly with drain-to-source voltage. Transient characteristics allowed determining the threshold voltage, values of which are cited in the preceding paragraph.

An analysis of magnetoconductivity of transistors presented below uses the following scheme. At low magnetic fields one observes a strong decrease of conductivity with an increase of the magnetic field which leads to a Lorentz-like shape of the magnetoconductivity curve. This curve is used for estimation of the electron mobility in the transistor channel. At large magnetic fields, Shubnikov–de Haas oscillations are observed and used for determination of the electron concentration. Measurements were performed for different values of the gate-to-source voltage. Results of measurements carried out on transistors are compared with magnetotransport results obtained for gated Hall-bars.
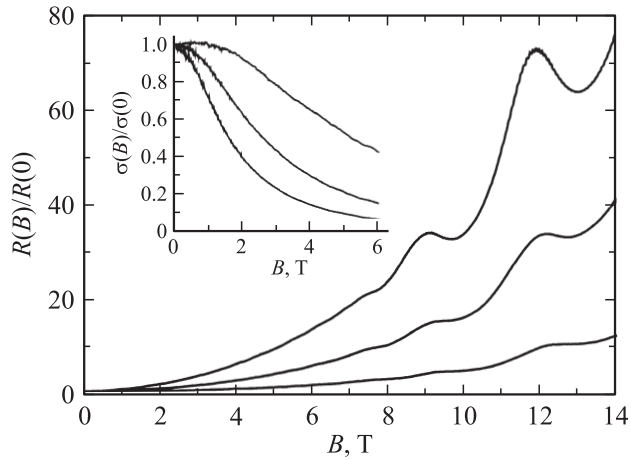
Figure 4. The resistance of a group *A* transistor, normalized at zero magnetic fild, for $U_{gs} = 0$, 0.2 and 0.3 V (from top to bottom). The unset shows normalized Lorenzian magnetoconductivity, $\sigma(B)$, curves characterized by decreasing μ for increasing U_{gs}.

Fig. 4 shows an example of a normalized drain-to-source resistance of a group *A* transistor vs. the magnetic field for a few values of the gate-to-source voltage. A background of these curves was fitted up to 4 T with a very high accuracy by a parabolic dependence, $1 + \mu^3 B^2$, with the mobility μ as a single fit parameter. We obtained μ equal to 0.60, 0.38 and 0.17 m^2/Vs for U_{gs} equal to 0, –0.2 and –0.3 V, respectively. This decrease of μ corresponds to a broadening of Lorentzian curves shown in the inset in Fig. 4, which present magnetoconductivity, $\sigma(B)$, normalised to its value at $B = 0$ T. The halfwidth of each Lorentzian, $B_{1/2}$, is given, of course, by an appropriate value of μ^{-1}. A simple inspection of the Shubnikov–de Haas oscillations in Fig. 4 shows that the number and position of maxima do not change with the applied gate-to-source voltage which means that in this transistor they are mainly due to the ungated part of the source-drain channel. The carrier density obtained from these oscillations (equal to $1.9 \cdot 10^{12}$ cm^{-2}) is expected to correlate with the carrier density in the transistor channel at the zero gate voltage. (It might be somewhat different depending on the values of the surface potential and of the gate contact built-in voltage.)

Let us concentrate now on measurements carried out on two transistors (T3 and T5 from group *B*). The transistors differed by the length of the gate, and the lateral dimension, which were equal to 2.5 and 55 μm for T3 and 1.5 and 25 μm for T5, respectively.

Fig. 5 shows the normalized magnetoconductivity for the transistors T3 and T5 for zero gate-to-source voltage. Lorentz-like curves show a strong decrease of the drain-to-source conductivity, σ, with an increase of the magnetic field. Curves of a similar shape were obtained for all gate-to-source voltages; they differ only in their halfwidth. The shape of magnetoconductivity curves is not strictly Lorentzian, in contrast to the curves shown in the inset in Fig. 4. This is illustrated by the inset of Fig. 5 which shows the square root of a transistor magnetoresis-

tance, $[R(B) - R(0)]^{1/2}$, normalized to its value at 1 T. If the magnetoconductivity were described by a Lorentzian $\left(1 + (B/B_{1/2})^2\right)^{-1}$, then this figure would show a straight line. We found that magnetoresistance for all gate-to-sourse voltages and for both transistors can be described by a Lorentzian-like dependence but with the exponent equal to 1.3 rather than 2. An inverse of the halfwidth of these Lorentzian-like magnetoconductivity curves, $B_{1/2}^{-1}$, is plotted as a function of a gate-to-source voltage in Fig. 6. This parameter, $B_{1/2}^{-1}$, of a dimension of mobility, decrease with increasing gate-to-source voltage for the transistor T5 (expect for a very small increase at lowest U_{gs}) and shows a mimimum for the transistor T5. The curves shown in Fig. 6 coincide for $U_{gs} < -0.3$, which for both transistors
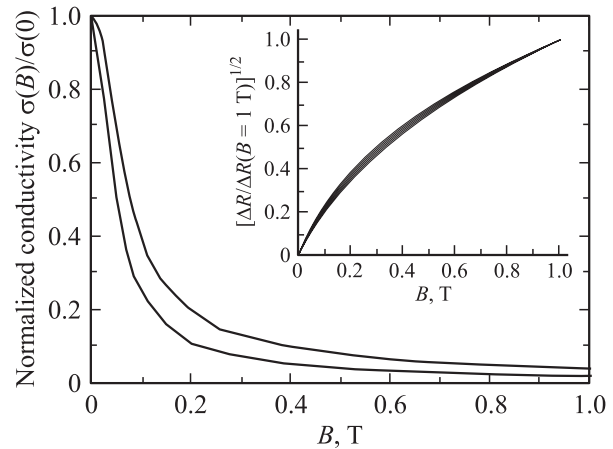

Figure 5. An influence of the magnetic field on conductivity for the transistor T3 (upper line) and T5 (lower line) — both transistors are from group *B*. The inset shows a square root of magnetoresistance $\Delta R = R(B) - R(0)$ of the transistors T3 and T5, normalised to its value at 1 T. The curves correspond to gate-to-source voltage equal (in Volts) to 0, –0.1, –0.2, –0.3, –0.4 for T5 and 0, –0.1, –0.2, –0.3 for T3.
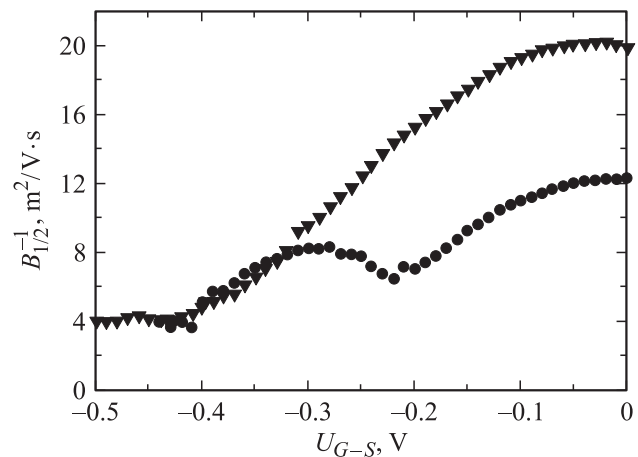

Figure 6. An inverse of the halfwidth of magnetoconductivity curves, $B_{1/2}^{-1}$, for the transistors T5 ($L = 1.5 \mu$m, down triangels) and T3 ($L = 2.5 \mu$m, solid circles), as a function of gate-to-source voltage, U_{gs}.

correspond to a drain current of about 20% of its value at the zero gate-to-source voltage.

Fig. 7 compares the conductivity of the transistors T3 and T5 (measured at $U_{gs} = 0\,\text{V}$) as function of the magnetic field — up to 7 T. After Lorentz-like behaviour at low fields, the oscillation of conductivity were observed. Taking into account the positions of minima of the magnetoconductance data, one can evaluate a concentration of the 2DEG, which appears to be $3.0 \cdot 10^{11}$ and $3.2 \cdot 10^{11}\,\text{cm}^{-2}$ for the transistors T3 and T5, respectively. One can note that the oscillations on the magnetoconductance curves are different from usual traces observed in the quantum Hall experiments. This is related to a difference in the samples geometry, which is Corbino-like for the case of the transistors. Gated Hall bar structures placed close to the transistors were used to perform a precise analysis of the influence of a gate-to-source voltage on the electron mobility and concentration in heterostructures used for transistor
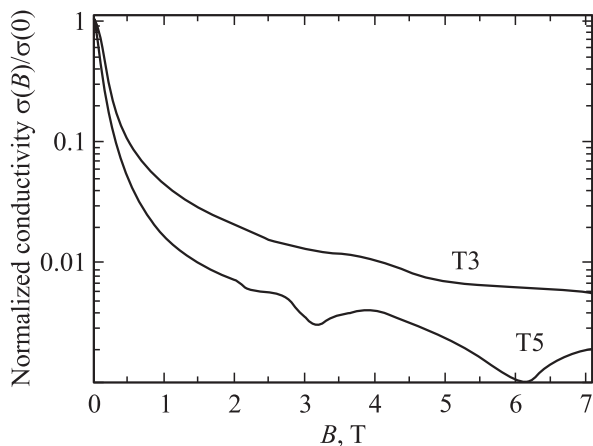

Figure 9. The electron mobility (squares) and concentration (down triangles) determined from measurements of the Hall effect on a gated Hall-bar of GaInAs/GaAlAs heterostructure from group *C*.

Figure 7. Magnetoconductance of the transistor T3 (upper curve) and T5 (lower curve).
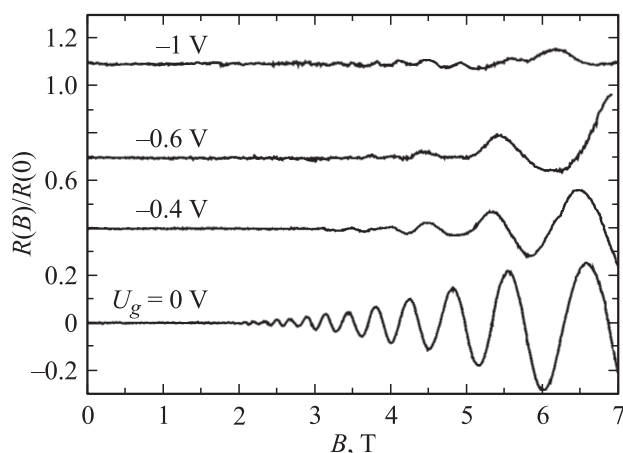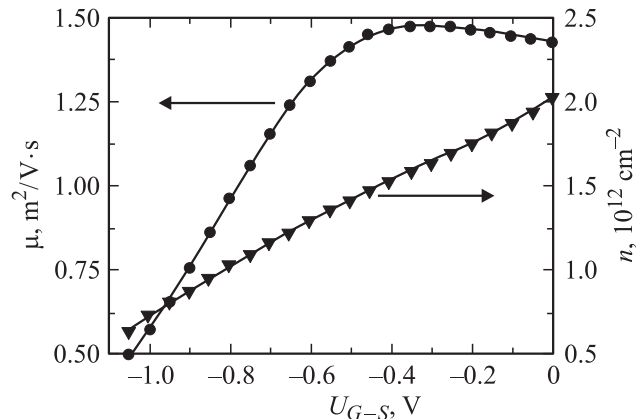

Figure 8. Shubnikov–de Haas oscillations of magnetoresistance of a Hall-bar processed out of GaInAs/GaAlAs heterostructure (group *C* of devices), as a function of the magnetic field, for gate potential equal to 0, 0.4, 0.6 and 1 V (from bottom to top). The curves are normalized at $B = 0\,\text{T}$ and shifted vertically for a better visualization.

fabrication. In Fig. 8 we show examples of results obtained on one of the Hall-bars placed together with the group (*C* — GaAs/GaInAs heterostructure). Fig. 8 shown the resistance values measured berween the Hall-bar probes as a function of the magnetic field. The curves were normalized to their value at $B = 0\,\text{T}$ and a monotonic background magnetoresistance was subtracted for a better visualization. The typical Shubnikov–de Haas oscillations were observed. The period (in B^{-1}) of the oscillations changes with decreasing the gate-to-source voltage swing, which corresponds to a decrease of the electron concentration. It is important to note, however, that not only the carrier density but also the mobility changes with inscreasing gate voltage — the amplitude of oscillation decreases and close to the threshold they are practically smeared out.

Fig. 9 summarizes the mobility and carrier density measurement results. As expected, the carrier density decreases linearly with application of a negative gate voltage. The linear extrapolation of the density versus gate voltage dependence to zero sheet density yields the threshold voltage equal to $U_{th} = -1.6\,\text{V}$. The threshold voltage obtained this way is different from the „transistor threshold" voltage — this point will be discussed later. The mobility first encreases slightly and then rapidly decreases with the gate voltage swing. Typically, we observed the mobility decrease by a factor of 2 to 3 at the gate voltage equal to half of the threshold voltage.

2. Discussion

The following discussion is divided into two parts. First, we consider a possibility of evaluating the electron concentration and mobility in the transistor channel basing on magnetoconductivity measurements. In view of this, we discuss the influence of geometry of investigated structures in the result of such a procedure. Also, the influence of the gate potential on the carrier density and

mobility in transistors and Hall-bars is discussed. Second, the electron mobility and concentration determined from magnetotransport measurements are used for interpretation of recently observed resonant detection and determination of the parameters of new field effect transistors processed for resonant detection of THz radiation.

The magnetoresistance measured between the source and the drain of the transistor is an integral phenomenon because of two effects i) comprises contributions from both the gated and the ungated part of a transistor channel and ii) channel geometry is often intermediate between Corbino and Hall-bar like.

The gated part of the channel (gate length) was $0.15\,\mu$m for the group A devices and 0.8–$2.5\,\mu$m for others. The total channel length was around $1\,\mu$m for group A devices and $10\,\mu$m for B and C groups. A clear evidence of the importance of the ungated part of the channel can be seen in Fig. 4 which shows Shubnikov–de Haas oscillations of the group A transistor. One can see that positions of maxima/minima do not depend on the gate-to-source voltage but the resistance of the transistor quickly grows with U_{gs}. This is because the oscillations come mainly from the $2D$ electron gas confined in the ungated part of the transistor. The background changes however — because the total resistance increases due to the modulation of the transistor channel by the gate voltage.

The mobility μ, determined as a coefficient of the parabolic dependence of resistance, corresponds to an „average" mobility in the entire region between the source and the drain. For the zero gate voltage the carrier densities in the gated and ungated regions of the channel are nearly the same. However, as it is clearly evidenced by measurements on the gated Hall-bars (where the whole conducting region is gated), a gate potential decreases both the mobility and the concentration of electrons (Fig. 9). We also expect that the mobilities in the gated and ungated sections of the device are close at zero gate bias, even though the scattering in the device channel might be affected by the effects related to the metal gate [18]. Once the gate voltage applied, the mobility under the gate is different from measured averaged mobility, since the mobility is a strong function of electron sheet density. With decreasing gate voltage swing, the resistance of the gated region starts to dominate the total transistor's resistance. In this case the measured (average) mobility approaches the value of mobility under the gate. Therefore, the measurements of magnetoresistance of the channel allow a relatively accurate determination of the mobility in the gated region for small gate voltage swings. In the intermediate region, one obtains the approximate „average" mobility. Comparison of Fig. 6 with Fig. 9 shows, however, that overall functional dependence of the mobility versus gate voltage in the transistor channel and in the gated Hall-bar are similar. The mobility decreases by a factor of 2–3 at the half of the threshold voltage.

Another point to be discussed is the conducting channel geometry. As mentioned in the introduction, the interpretation of the transistor magnetoresistance is simple if the conducting channel geometry approaches the limiting case of the Corbino geometry. This condition is fulfilled for a „very wide channel" — with the source-to-drain separation length, I_c, being much smaller than the channel width, D. In this case, the magnetoresistance is parabolic (or the magnetoconductance is Lorentzian). Such a parabolic ($R \sim 1 + \mu^2 B^2$) behaviour was observed for group A transistors (gate of $0.15\,\mu$m) that have a very short ($L_c \sim 1\,\mu$m) and wide ($d \sim 50\,\mu$m) channel.

For transistors T3 and T5 D/L_c ratio is 5.5 and 2.5, respectively, and the geometry is neither Corbino nor a Hall-bar type. We speculate that the observed exponent of 1.3 is related to the fact that the geometry of the current flow is far from the ideal cases presented above. In particular, an essential part of the current may flow outside of the transistor due to violation of the condition $j_y = 0$. Nevertheless, and in spite of difficulties in interpretation mentioned above, one can consider the parameter $B_{1/2}^{-1}$ as an estimate of the electron mobility. This interpretation is consistent with the behaviour of two curves shown in Fig. 6, which coincide for higher gate-to-source voltage, close to the threshold value ($U_{gs} < -0.3\,$V), when the transistor resistance is determined by the gated section. The fact that we find the same exponent (equal to 1.3) for both transistors confirms that although determination of the electron mobility as $B_{1/2}^{-1}$ is an approximation, it can be used to compare the electron mobility in different transistors.

It is important to note that both mobility obtained on gated Hall-bars (shown in Fig. 9) and the mobility extracted using $B_{1/2}^{-1}$ values for ghe transistors (shown in Fig. 6) decrease with decreasing the gate-to-source voltage swing. This might be is linked to the screening effects that diminish at smaller electron sheet densities. This decrease reduces the effectiveness of screening of ionised centres and results in a decrease of the mobility. The application of the gate voltage also changes the shape of the quantum well at the heterointerface. The quantum well is wider at smaller sheet densities. Hence, the peak of the $2D$ electron wavefunction is further away from the heterointerface, which decreases scattering by the interface roughness. This effect can lead to a mobility increase. It is possible that the non-monotonic behaviour of $B_{1/2}^{-1}$ observed for both transistors (close to zero gate — source voltage for T5 and at about –$0.2\,$V for T3) and for the Hall-bar at around –$0.4\,$V can be attributed to the interplay of these two mechanisms.

Measurments of the carrier density and mobility made on the gated Hall-bars also show that the threshold voltage for the carrier density and for the channel conductivity can be fairly different. From the linear approximation of the carrier density versus gate dependence shown in Fig. 9 we obtained the threshold voltage (voltage for which the carrier density is zero) equal to $U_{th} = -1.6\,$V. If we use the same procedure for conductivity, the threshold voltage of $U_{th} = -1.4\,$V is obtained. This is because both the carrier density and mobility enter into conductivity and both decrease with an increase of the gate voltage. It is important to note that the threshold that in estimations of the plasma wave frequency is the carrier density threshold.
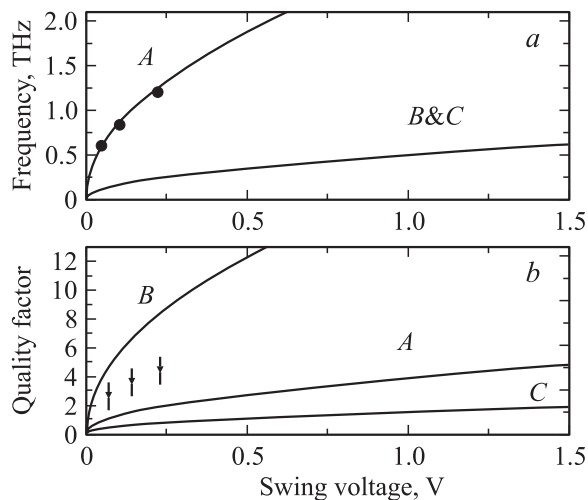
Figure 10. *a* — frequency of the resonant detection of the group *A*, *B* and *C* transistors, as a function of the swing voltage. *b* — quality factor corresponding to a frequency of the resonant detection, plotted in *a*), for the group *A*, *B* and *C* transistors.

Using the value of the mobility and the threshold voltage determined for different FET's we can estimate their parameters for possible applications in the resonant detectors of the terahertz radiation. In Fig. 10, we show the frequency of the resonant detection and the quality factor as a function of the swing voltage. The maximum frequency for a detector is determined by the maximum gate voltage swing and the gate length. As discussed before, the maximum gate voltage swing is determined by „the carrier density threshold voltage". It is usually slightly more negative than the transistor threshold voltage. The maximum gate voltage swing is about $0.5\,\mathrm{V}$ for the group *A* and *B* transistors and $1.5\,\mathrm{V}$ for the group *C*. We took gate length $L = 0.15\,\mu\mathrm{m}$ for the group *A* and $L = 0.8\,\mu\mathrm{m}$ (shortest gates on a dice) for the group *B* and *C*. The mobility was assumed to be 6, 14 and $1\,\mathrm{m^2/Vs}$ for the group *A*, *B* and *C*, respectively.

As can be seen from the figure, the maximum frequency of the group *A* devices is approximately $1.5\,\mathrm{THz}$. The points shown in Fig. 10 represent the results of recent experiments [14,15]. The plasma resonance observed in the experiments were relatively weak (Fig. 1). This can be understood by looking at the figure presenting the quality factor. One can see that the maximum quality factor that can be obtained for these devices is around 1.5. The reason for this is the relatively low mobility. For the group *C*, the maximum frequency is $0.6\,\mathrm{THz}$. The maximum quality factor for this frequency is relatively small, equal to about 2. It means that these devices can not be used for resonant tuneable detection. The best quality factors were obtained for group *B* transistors. At the maximum operation frequency $0.35\,\mathrm{THz}$ (corresponding to the maximal swing voltage of $0.5\,\mathrm{V}$) the quality factor for these devices is larger than 10. These are the most promising devices for high quality resonant plasma detectors.

In principle, the simplest way to increase the maximum frequency (and the quality factor) is to decrease the gate length (L) — see Eq. 1. The shortest gate length (L_{min}) for a given type of devices can bi defined by an approximate relation $L_{min} \sim 5d$ where d is the gate to channel distance (in order to preserve the gate control). Looking at the dimensions of the three groups of devices one can see that the devices of group *A* ($d \sim 0.025\,\mu\mathrm{m}$, $L \sim 0.15\,\mu\mathrm{m}$) and *B* ($d \sim 0.16\,\mu\mathrm{m}$, $L \sim 0.8\,\mu\mathrm{m}$) are close to the limit. Only the heterostructures used for group *C* devices ($d \sim 0.04\,\mu\mathrm{m}$, $L \sim 0.8\,\mu\mathrm{m}$) can be used for fabricating shorter gate length transistors. The minimum gate length for these transistors is approximately $0.2\,\mu\mathrm{m}$. One can expect then to reach the maximum detection frequency of about $2.4\,\mathrm{THz}$ with a maximal quality factor of about 6.

In conclusion, transistors processed from GaAs/GaAlAs and GaInAs/GaAlAs heterostructures were investigated by magnetotransport measurements in order to characterize their applicability as resonant tuneable detectors of THz radiation. We showed how the electron mobility in the transistor can be evaluated from a magnetic field dependence of the transistor's resistance. High-mobility GaAs/GaAlAs transistors with a quality factor approaching 10 were fabricated. These devices are most promising (among those investigated) devices for application as resonant detectors.

References

[1] A.C. Samuels, D.L. Woolard, T. Globus, B. Gelmont, E.R. Brown, J.O. Jensen, R. Suenram, W.R. Loerop. Environmental Sensing of Chemical and Biological Warfare Agents in the THz Region. WOFE-02 Proceedings. Yoon Soo Park / Ed. by Michael S. Shur, William Tang. (2002).

[2] B. Ferguson, X.-C. Zhang. Nature Materials **1**, 26 (2002).

[3] M. Kroug, S. Cherednichenko, H. Merkel, E. Kollberg, B. Voronov, G. Gol'tsman, H.W. Huebers, H. Richter. IEEE Transactions on Applied Superconductivity **11**, 962 (2001).

[4] P.J. Burke, R.J. Schoelkopf, D.E. Prober, A. Skalare, B.S. Karasik, M.C. Gaidis, W.R. McGrath, B. Bumble, H.G. LeDuc. J. Appl. Phys. **85**, 1644 (1999).

[5] B.S. Karasik, W.R. McGrath, M.E. Gershenson, A.V. Sergeev. J. Appl. Phys. **87**, 7586 (2000).

[6] T.W. Crow, R.J. Mattauch, R.M. Weikle, U.V. Bhapkar. In: Compound Semiconductor Electronics / Ed. by M. Shur. World Scientific Publishing (1996). P. 209.

[7] S.M. Marazita, W.L. Bishop, J.L. Hesler, K. Hui, W.E. Bowen, T.W. Crowe. IEEE Transaction on Electron Devices **47**, 1152 (2000).

[8] E.E. Haller, J.W. Beeman. In: Proceedings of Far-IR, Sub-mm & mm Detector Technology Workshop, April 2002, Monterey, CA, in press.

[9] G.E. Stillman, C.M. Wolfe, J.O. Dimmock. Solid State Commun. **7**, 5 (1969).

[10] W. Knap, J. Lusakowski, K. Karpierz, B. Orsal, J.L. Robert. J. Appl. Phys. **72**, 680 (1992).

[12] For review see M. Dyakonov, M.S. Shur. In: Terahertz Sources and Systems / Ed. by R.E. Miles. Kluwer Academic Publ., Netherlands (2001). P. 187.

[13] M. Dyakonov, M.S. Shur. Phys. Rev. Lett. **71**, 2465 (1993); IEEE Trans. on Elec. Dev. **43**, 380 (1996); Proc. of 22nd Int. Symp. on GaAs and Related Compounds. Institute Conf. Ser. (1996). N 145. Ch. 5. P. 785.

[14] W. Knap, Y. Deng, S. Rumyantsev, J.-Q. Li, M.S. Shur, C.A. Saylor, L.C. Brunel. Appl. Phys. Lett. **80**, 3433 (2002).

[15] W. Knap, Y. Deng, S. Rumyantsev, M.S. Shur. Appl. Phys. Lett. **81**, 4637 (2002).

[16] X.G. Peralta, S.J. Allen, M.C. Wanke, N.E. Harff, J.A. Simmons, M.P. Lilly, J.L. Reno, P.J. Burke, J.P. Eisenstein. Appl. Phys. Lett. **81**, 1627 (2002).

[17] W. Knap, V. Kachorovskii, Y. Deng, S. Rumyantsev, J.-Q. Li, R. Gaska, M.S. Shur, G. Simin, X. Hu, M. Asif Khan, C.A. Saylor, L.C. Brunel. J. Appl. Phys. **91**, 9346 (2002).

[18] A.A. Grinberg, M.S. Shur. J. Appl. Phys. **58**, 382 (1985).